coatings

Article

Metamaterial Solar Absorber Based on Refractory Metal Titanium and Its Compound

Zijun Song [1,2], Guolu Ma [3,*], Zao Yi [3], Jianguo Zhang [4,*] and Yong Zhao [1]

1 Aviation Key Laboratory of Science and Technology on Altitude Simulation, Mianyang 621700, China; 15280939727@163.com (Z.S.); yong_zhao@yeah.net (Y.Z.)
2 Department of Engineering Mechanics, Tsinghua University, Beijing 100084, China
3 Key Laboratory of Manufacturing Process Testing Technology of Ministry of Education, Joint Laboratory for Extreme Conditions Matter Properties, Southwest University of Science and Technology, Mianyang 621010, China; yizaomy@swust.edu.cn
4 Department of Physics, Jinzhong University, Jinzhong 030619, China
* Correspondence: maguolu999@163.com (G.M.); phys.zhangjg@gmail.com (J.Z.); Tel./Fax: +86-0816-2480830 (G.M.)

Abstract: Metamaterials refers to a class of artificial materials with special properties. Through its unique geometry and the small size of each unit, the material can acquire unique electromagnetic field properties that conventional materials do not have. Based on these factors, we put forward a kind of high absorption near-ultraviolet to near-infrared electromagnetic wave absorber of the solar energy. The surface structure of the designed absorber is composed of TiN-TiO_2-Al_2O_3 with rectangles and disks, and the substrate is Ti-Al_2O_3-Ti layer. In the study band range (0.1–3.0 μm), the solar absorber's average absorption is up to 96.32%, and the designed absorber absorbs more than 90% of the electromagnetic wave with a wavelength width of 2.577 μm (0.413–2.990 μm). Meanwhile, the designed solar absorber has good performance under different angles of oblique incident light. Ultra-wideband solar absorbers have great potential in light absorption related applicaitions because of their wide spectrum high absorption properites.

Keywords: surface plasmons; solar absorber; metamaterials; FDTD method

check for updates

Citation: Song, Z.; Ma, G.; Yi, Z.; Zhang, J.; Zhao, Y. Metamaterial Solar Absorber Based on Refractory Metal Titanium and Its Compound. *Coatings* **2022**, *12*, 929. https://doi.org/10.3390/coatings12070929

Academic Editor: Anna Palau

Received: 16 June 2022
Accepted: 28 June 2022
Published: 30 June 2022

1. Introduction

Metamaterials were proposed in the nineties of the 20th century [1]. They have some special properties such as changing the interaction of light or electromagnets with the matter, but the materials made by traditional methods can not implement it. Metamaterials are nothing special in the composition of matter, and their peculiar properties are due to their unique geometry and the small size of each unit. When the scale of the microstructure is close to the incident wavelength, the influence on the wave can be realized [2]. In the last 10 years, the absorber based on meta-material developed rapidly [3–7]. At the same time, many researchers have also made very significant contributions in the manufacturing process of metamaterials, such as Akinoglu et al. who report their research on BCP (block copolymer) lithography route [8,9]. Landy et al. proposed a metamaterial that can efficiently absorb electromagnetic radiation, with a wide absorption bandwidth and polarization insensitivity [10]. These absorbers achieving high absorption of light can effectively convert solar energy into heat energy, which is important for utilizing solar energy for people [11–15]. In addition, the absorbers based on meta-materials and surface plasmon materials have significant application in a variety of multispectral applications, such as photon detection, spectrum sensing, photocatalysis, etc. [16–23].

Precious metals were widely used in solar absorber because of their plasmon resonance and optical coupling behavior [24,25]. Wu et al. designed a solar absorber based on precious metals, absorption of which is more than 90% in wavelength range of 0.4 μm to 2 μm [24].

However, due to plasma nano-signal resonance characteristics of precious metals, multiple layers are required to have an ideal effect. At the same time, the high cost of precious metals improved the budget for making absorbers. Thus, refractory metals and their compounds have received great attention because of their large imaginary part of the dielectric constant, which can cause huge losses to electromagnetic waves [25–29]. Besides, refractory metals have high melting points and are resistant to acids and alkalis. Titanium is a refractory metal with a melting point as high as 1660 °C, and its compound also has a high melting point. Therefore, they can work under high temperatures normally. Compared to precious metal, titanium's larger reserves also result in lower costs. Thus, we can say refractory metals and their compounds have great potential for application in solar absorbers [30–32].

In this paper, we designed a solar absorber based on Ti and its compounds. According to the reasonable design and parameter of structure, the designed absorbers that achieve ultra-wideband high absorption to solar raditation. We verify the results by simulating the solar absorber with FDTD. Design of the absorber within the study band performance is good. The absorption of the designed absorber is higher than 90% in wavelength range of 2.577 μm (0.413–2.990 μm). The designed absorber's average absorption is up to 96.32% in the researched band (0.1–3.0) μm. Meanwhile, we evaluate its real performance by simulating the performance of the designed absorber under the real solar spectrum. Then, we discuss the influence of changes to geometrical parameters and various parts of the absorber on the performance of the absorber, and explore its absorbing mechanism. Last, the designed solar absorber can realize ultra-wideband high absorption, which fulfills the requirement of solar cells, thermo-photovoltaics, and thermal radiation [33,34]. Besides, small thickness of the designed absorber is one of advantages. Thus, the proposed meta-surface as a coating of solar cells is a direction worth considering [35,36].

2. Structural Design of Absorber with Wide Spectrum and High Absorption

The structure of the designed solar absorber is shown in Figure 1a. The substrate of the absorber is a Ti-Al_2O_3-Ti three-layer structure, and its surface structure is composed of disks and rectangles of TiN-TiO_2-Al_2O_3. The front view of the absorber is shown in Figure 1b. The period of each unit is T = 0.4 μm, and the surface of each period is composed of four groups of equally sized bars of Ti-Al_2O_3-Ti. W = 0.06 μm and L = 0.21 μm are the width and length of the strip structure, respectively. The disk structure is located in the center of the absorption unit of the absorber, which is also composed of TiN-TiO_2-Al_2O_3 and has a radius of R = 0.06 μm. H_1 = 0.08 μm, H_2 = 0.105 μm and H_3 = 0.05 μm are the heights of TiN, TiO_2 and Al_2O_3 layers, respectively. H_4 = 0.025 μm, H_5 = 0.125 μm and H_6 = 0.275 μm are the thickness of the top Ti layer, Al_2O_3 layer and bottom Ti layer of the substrate, respectively.

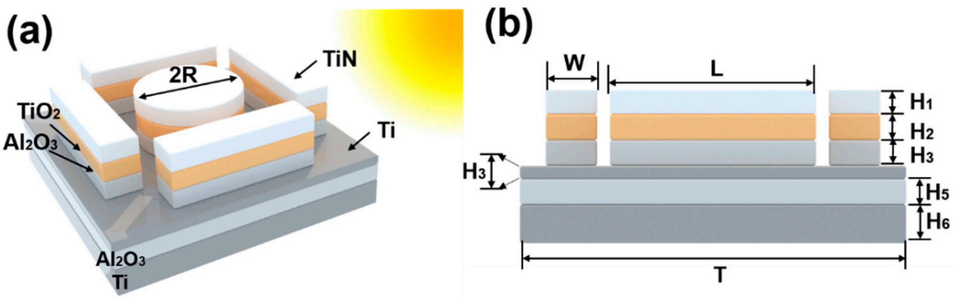

Figure 1. (**a**) The principle diagram of the ultra-broadband solar energy absorber. (**b**) Front view of the absorber.

For simulating the absorption performance of the absorber, we adopt the FDTD (Finite Difference Time Domain) method to simulate the designed solar absorber [37–39]. We use plane light of wavelength of 0.1 μm to 3.0 μm illuminated from above the Z axis of the absorber, and simulating the actual scattering of electromagnetic waves by using PML (Perfect Match Layer) boundary conditions above Z direction outside the structural region.

In X and Y direction, we adapt period boundary condition to reproduce the array pattern of the designed absorber. We place the detector on the bottom and above the absorber to measure the transmission (T) and reflection (R) of the absorber, respectively. Absorption (A) = 1 − T − R [40–43]. The TiO_2, Ti, TiN and Al_2O_3 used in simulation calculation come from Palik [44].

3. Simulation Results and Discussion

Figure 2a shows the reflection (R), transmission (T) and absorption (A) spectrum diagram of designed solar absorber in normally incident electromagnetic wave. In whole researched wavelength (0.1–3.0 µm), the range wavelength of absorption is higher than 90% at 2.577 µm, and the average absorption is 96.32%. At the same time, the absorption reached 95.6%, 99.45% and 98.97% in the absorption peak at λ = 0.4442 µm, 0.8407 µm and 1.7294 µm, respectively. Due to the goal of designing a solar absorber that absorbed solar radiation, we study the absorption of solar radiation by the designed absorbers. The absorption spectrum of the absorber under AM1.5 spectrum is shown in Figure 2b. The AM1.5 spectrum refers to the atmospheric mass of AM1.5 when θ = 48.2°. This refers to a typical sunny day when the sun's rays illuminate the general ground, which is closer to the actual situation of human life, and its irradiance is 1000 W/m^2. AM 1.5 is often used as the incident light energy standard to evaluate the performance of ground-based solar energy conversion devices and modules [45]. We can see the energy of solar radiation is concentrated in the near-ultraviolet to near-infrared. Thus, the designed absorber must be within the scope of the electromagnetic wave that has high absorption ability, to realize the strong absorption of solar energy absorber. According to Figure 2b, the designed absorber only has a small amount of energy loss in near-ultraviolet to near-infrared in the solar energy's absorption, so the designed absorber has a good performance under AM1.5 sunlight. According to Figure 2, we know the designed absorber has good performance in solar absorption. In Table 1, we also compared several reported solar absorbers to show that the advantage of the designed absorber.

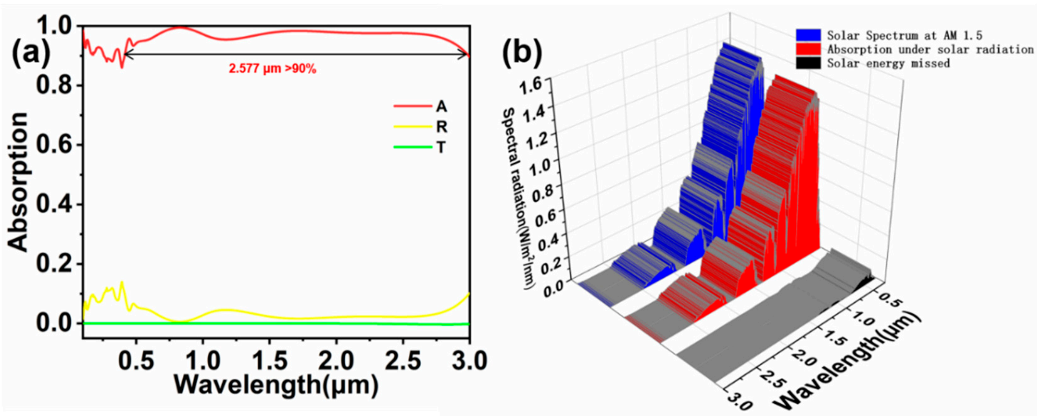

Figure 2. (**a**) the reflection (R), transmission (T) and absorption spectra of the solar absorber designed for normal incidence; (**b**) absorption effect under AM1.5 spectrum.

Table 1. Absorption range of different structures with an absorption rate of more than 90%.

Reference	Structure	Absorption Range	Wavelength Range with Absorption More than 90%	Average Absorption
This work	Ti-Al_2O_3-Ti	0.413–2.990 µm	2.577 µm	96%
[46]	TiN and TiO_2 disk	0.316–1.426 µm	1.11 µm	93%
[47]	Si–Cr–Al three-layer	0.4–1.8 µm	1.4 µm	97%
[48]	SiO_2-Ti-MgF_2-Al	0.405–1.505 µm	1.1 µm	95.14%

Then we try to research the physical mechanism of absorption of solar radiation by absorbers. The designed absorber is strongly coupled with incident light in several wavelengths, which results in the absorption peaks appearing in spectrum. Thus, we can research the physical mechanism of absorption by simulating and analyzing the electric field contribution of the absorber at absorption peak. The results are shown in Figure 3. In Figure 3a,b, electricity is mainly limited in the top disk and surface of rectangle at λ = 0.4442 µm. The scattering between adjacent structures is strongly suppressed, and the field at the gap is highly localized. The LSPR (Localized Surface Plasmon Resonance) excited makes the main contribution to the absorption at this wavelength [49–51]. Figure 3b,f show the electric diagram of the absorption peak at λ = 0.8407 µm. We can find that the electric field is mainly concentrated in the middle disk structure of the surface structure at this wavelength. Similarly, the electric field being bound to the disks on the surface indicates that the LSPR is excited, and at the interface between the bottom of the middle disk and the bottom disk, the electric field is constrained in the vertical direction and decays rapidly. The SPPs (Surface Plasmon Polaritons) are excited by a coupling of electromagnetic and electron plasma oscillations in the material [52–54]. The electric field distribution in Figure 3c,d,g,h is similar to Figure 3b,f. The difference is that the absorption peak at the wavelength λ = 1.7294 µm and the electric field at the long wavelength band λ = 2.7100 µm are also distributed between the gaps of adjacent unit structures. This part of the LSRP enhances the absorption capacity of the long wavelength band. Because of these factors, the designed solar absorber has good performance in the whole band.

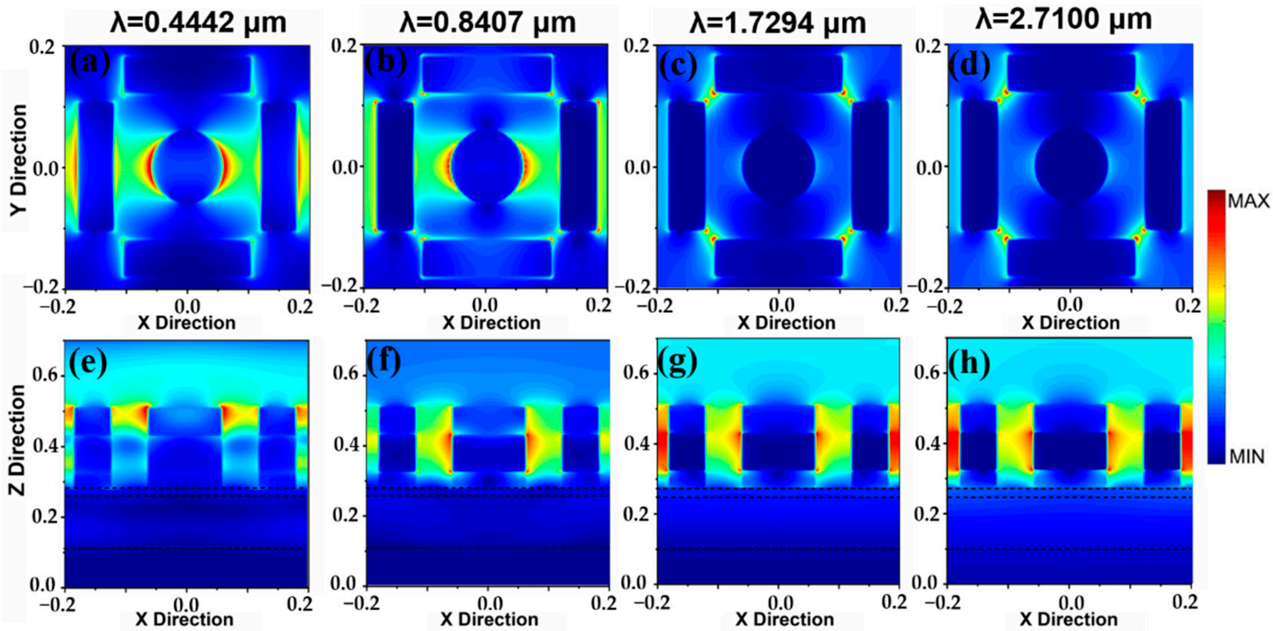

Figure 3. Simulated electric field diagrams. (**a**) X-Y plane at λ = 0.4442 µm; (**b**) X-Y plane at λ = 0.8407 µm; (**c**) X-Y plane at λ = 1.7294 µm; (**d**) X-Y plane at λ = 2.7100 µm; (**e**) X-Z plane at λ = 0.4442 µm; (**f**) X-Z plane at λ = 0.8407; (**g**) X-Z plane at λ = 1.7294 µm; (**h**) X-Z plane at λ = 2.7100 µm.

To research the influence of structural parameters changed on absorber, we try to adjust the surface structure's parameters. The simulation results are shown in Figure 4a; changing the disk's radius of structure does not have significant effect on the absorption spectrum of the absorber because it has less electric field distribution in the gap between disk and rectangle structure. Figure 4b show the absorption spectrum with changing the width of rectangles. Each absorption peak is generated by the strong coupling between incident photon and material. In Figure 3, we analyze the electric field distribution diagram of each coupling absorption peak. Because the electric field is mainly localized between adjacent units, LSPR excited and SPP excited between adjacent rectangles are formed. Therefore, changing the width of W will have a great influence on the coupling band and intensity.

With the increase in W, the effect on the long wavelength is most significant. The absorption peak of the long wavelength appears to have a red shift, and the resonance absorption peak of 1.7 μm disappears gradually, while the resonance intensity of the absorption peak of 2.7 μm becomes stronger. When W exceeds 0.07 μm, the absorption of electromagnetic waves by the absorber decreases rapidly because the excitation mode begins to change. We change the length of the rectangle W in Figure 4c. We predict that the absorption near $\lambda = 0.4442$ μm will not be greatly affected in the short-wave band because the intensity of the excited SP (surface plasmon) has little correlation with the length of the rectangular structure in the band [55,56]. In the long wave band, the intensity of SP excitation is obviously affected by the length of L, so the absorption spectrum of the long-wave band will have obvious changes in the change of L. The resonant absorption peaks ($\lambda = 1.7$ μm and $\lambda = 2.7$ μm) show red shift and intensity change with the increase in L. In Figure 4d, what has changed is the size of the period T of the absorber absorption unit. By changing the parameter of the period T, we can foresee the greatest impact on the surface plasmons excited between adjacent cells. We can see that for the long wavelength band where the absorption is very dependent on the local surface plasmon resonance, even if the amplitude of T is changed in a very small range, the effect on the absorber's absorption spectrum is significant [57].

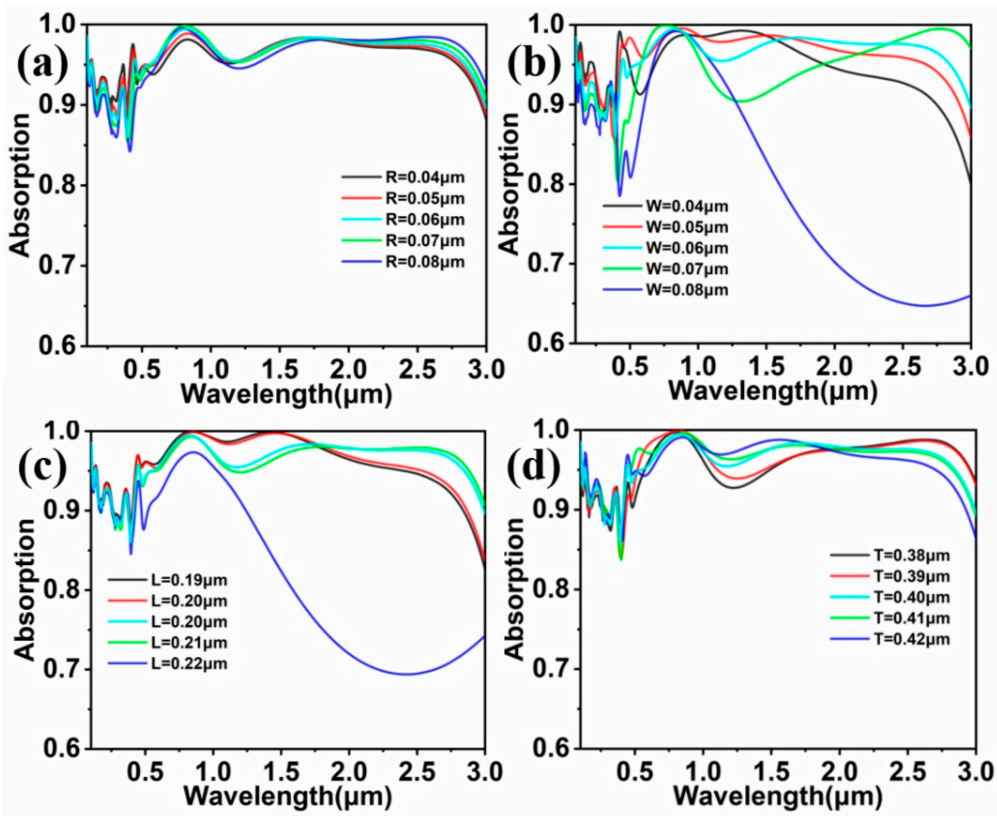

Figure 4. The simulated absorption spectrum of the designed absorber after changing the structural parameters of the surface. (**a**) Absorption spectra at different R; (**b**) Absorption spectra at different W; (**c**) Absorption spectra at different L; (**d**) Absorption spectra at different T.

In order to further investigate the changes in the absorber's absorption spectrum, Figure 5 shows the simulated spectrum of designed absorber when the thickness of the surface structure was changed. The changing of H_1 has a significant impact on absorption in the middle band. When the H_1 thickens, the intensity of absorption peak in the middle band is weak and appears to show redshift. At the same time, the absorption between $\lambda = 1$ μm and 1.25 μm decreases. Through Figure 3, we know the mode of exciting surface plasmon is the difference of absorption peak at $\lambda = 0.4442$ μm and absorption peak at $\lambda = 0.8407$ μm. We can infer that the adjacent widened absorption peaks are superimposed to achieve high absorption between λ = 1 μm and 1.25 μm. The thickness of the TiO_2 layer is changed in Figure 2b. The intensity of absorption peak increases. However, the absorption peak at λ = 0.8407 μm starts blueshift and at λ = 1.7294 μm shows redshift. The tearing of adjacent absorption peaks leads to a rapid decrease in the absorption between λ = 1 μm and λ = 1.25 μm. Figure 5c shows the spectrum with changing H_3. The phenomenon and reasons are similar to those in Figure 5b. Through the analysis of Figures 4 and 5, it can be concluded that we can manually adjust the absorber's absorption spectrum by adjusting the geometric parameters.

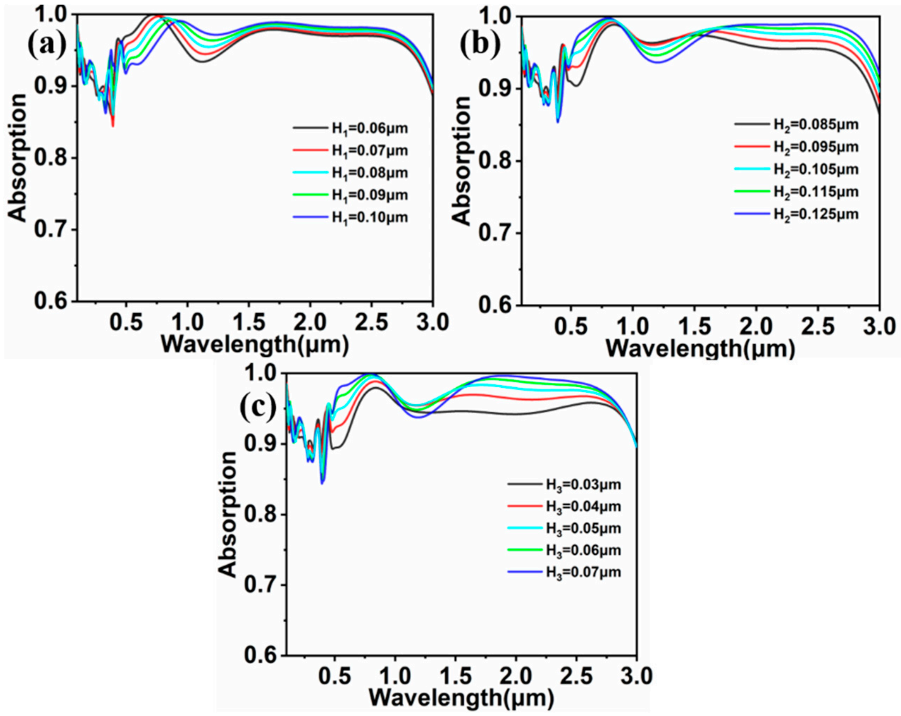

Figure 5. Simulated absorption spectrograms of the thickness parameter variation of the designed absorber surface structure. (**a**) Absorption spectra at different H_1; (**b**) Absorption spectra at different H_2; (**c**) Absorption spectra at different H_3.

For natural incident light, it has many polarition directions at once [58–60]. The solar absorber with high absorption to various polarization directions of electromagnetics is important [61]. When the incident light changes from TM polarized light to TE polarized light, the spectrum of the absorber is shown in Figure 6a. Excited surface plasmon is usually easily affected by changes in the polarization angle, but because the surface structure of the designed absorber is symmetrical, it is not affected by the polarization angle. It is also worth considering when electromagnetic waves are incident through a certain angle, and the result is shown in Figure 6b. With the incident angle increasing, there are cases where the width of the high-absorption band gradually decreases. The absorber has an ideal effect on the absorption spectrum where the incident light angle is less than 50°, which can meet the needs in most cases. Therefore, the designed absorber can be applied to devices operating in natural light [62–65].

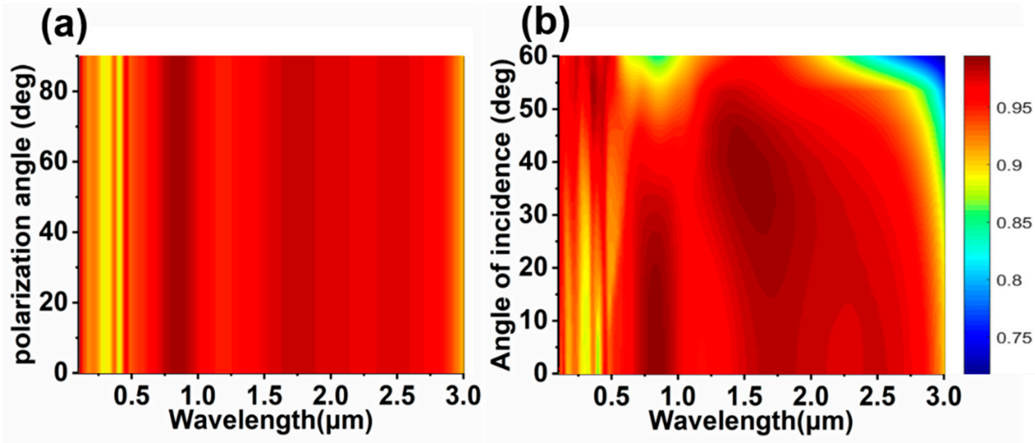

Figure 6. (**a**) The simulated absorption spectra of the designed absorber in TM polarization to TE polarization state and (**b**) the simulated absorption spectrum under the condition of oblique incidence.

In order to further verify the effect of each part on the absorber, we explore the influence of substrate structures on the spectrum of designed absorber in Figure 7a. After removing the titanium in the uppermost layer of the substrate and the aluminum oxide in the middle layer, the absorber's ability to absorb electromagnetic waves has been significantly reduced. Although fewer electric fields contribute to the substrate of the absorber, it is important to excite and enhance surface plasmon resonance [66,67]. In Figure 7b, we explore the impact of different surface structure on the absorber's absorption spectrum. The situation A is that the disk in the center is removed. The absorption of the absorber decreases in visible bands, and absorption band narrows but still has good performance. It indicates we can adapt a simple structure to meet the requirement when the absorption rate is not strict. In situation B, the rectangles in the surface structure are canceled. And the absorption of the absorber declines rapidly, especially in mid-band and long-band. This phenomenon can also be foreseen from the electric field diagram in Figure 3. Most of the electric fields are distributed on the surface of the rectangle structure or between adjacent strip structures, so the rectangle structure plays a very important role in the absorption of the absorber [68]. Finally, we explore the contribution of substrate structure to absorption in situation C. The absorber has low absorption to the electromagnetic especially in visible-band. Thus, the substrate needs to work with the surface structure to achieve wide spectrum and high absorption.

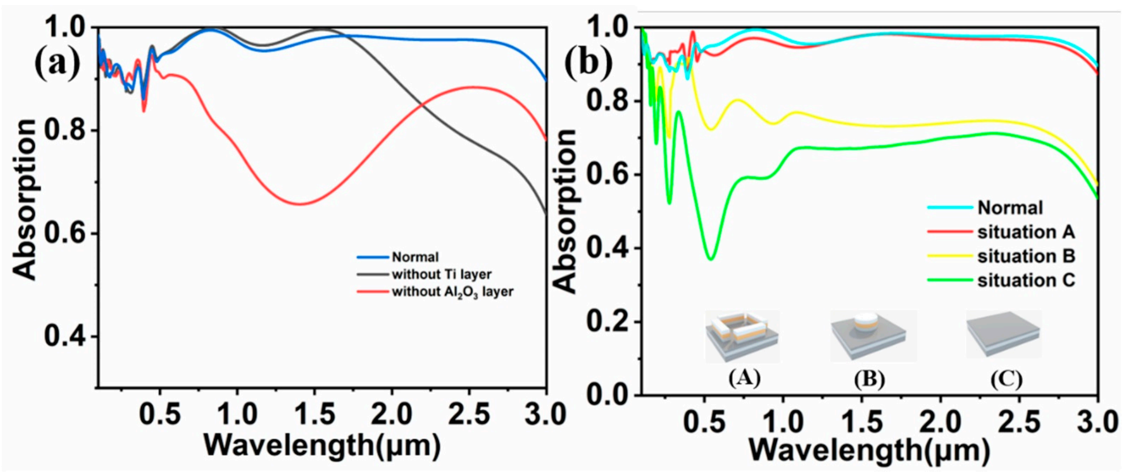

Figure 7. The simulated absorption spectra under different substrates (**a**) and simulated spectra of different surface structures (**b**).

4. Conclusions

In this paper, we designed a new structure of solar absorber based on refractory metals, the basic unit structure of which includes a substrate composed by Ti-Al_2O_3-Ti, four rectangles and a disk of TiN-TiO_2. According to the suitable geometry structure and parameters, the designed solar absorber achieves high absorption of solar energy. The absorber's average absorption is 96.32%. In the whole research of the wavelength band (0.1–3.0 μm), the wavelength range of the absorption is higher than 90%, as wide as 2.577 μm (0.413–2.990 μm). We discussed its physical mechanism more systematically from the principle and electric field distribution. Afterwards, we discussed the structure through the adjustment of geometric parameters to artificially directionally control the absorber's absorption spectrum, as well as the influence of the polarization angle and incident angle on the performance of the solar absorber. In summary, we believe that the designed absorber in this article has broad application prospects in light-to-heat conversion equipment, solar power generation, and optical filtering.

Author Contributions: Conceptualization, Z.S., G.M. and Z.Y.; data curation, Z.S., G.M. and J.Z.; formal analysis, Z.S. and Y.Z.; methodology, Z.S., G.M., Z.Y. and Y.Z.; resources, Z.S.; software, Z.S. and Y.Z.; data curation, Z.S.; writing-original draft preparation, Z.S.; writing-review and editing, Z.S., G.M., Z.Y. and J.Z. All authors have read and agreed to the published version of the manuscript.

Funding: The authors are grateful to the support by National Natural Science Foundation of China (No. 51606158, 11604311, 61705204, 21506257); the Funded by the Scientific Research Fund of Si Chuan Provincial Science and Technology Department (2020YJ0137; 2020YFG0467; 2021JDRC0019); the Funded by the Open Fund of The Key Laboratory for Metallurgical Equipment and Control Technology of Ministry of Education in Wuhan University of Science and Technology (No. MECOF2020B02); the Funded by the Undergraduate Innovation Fund Project Precision Funding by Southwest University of Science and Technology (No. JZ20-025); the Postgraduate Innovation Fund Project by Southwest University of Science and Technology (No. 18ycx034); the Funded by Southwest University of Science and Technology Students Innovation Fund project (No. CX20-031).

Institutional Review Board Statement: Not applicable.

Informed Consent Statement: Not applicable.

Data Availability Statement: Publicly available datasets were analyzed in this study. This data can be found here: [https://www.lumerical.com/].

Conflicts of Interest: The authors declare no conflict of interest.

References

1. Smith, J.R. Range scaling of wirelessly powered sensor systems. In *Wirelessly Powered Sensor Networks and Computational RFID*; Springer: New York, NY, USA, 2011; pp. 3–12.
2. Chen, J.; Nie, H.; Tang, C.J.; Cui, Y.H.; Yan, B.; Zhang, Z.Y.; Kong, Y.R.; Xu, Z.J.; Cai, P.G. Highly sensitive refractive-index sensor based on strong magnetic resonance in metamaterials. *Appl. Phys. Express* **2019**, *12*, 052015. [CrossRef]
3. Zheng, Z.P.; Luo, Y.; Yang, H.; Yi, Z.; Zhang, J.G.; Song, Q.J.; Yang, W.X.; Liu, C.; Wu, X.W.; Wu, P.H. Thermal tuning of terahertz metamaterial properties based on phase change material vanadium dioxide. *Phys. Chem. Chem. Phys.* **2022**, *24*, 8846–8853. [CrossRef]
4. Jiang, L.; Yi, Y.; Tang, Y.; Li, Z.; Yi, Z.; Liu, L.; Chen, X.; Jian, R.; Wu, P.; Yan, P. A high quality factor ultra-narrow band perfect metamaterial absorber for monolayer molybdenum disulfide. *Chin. Phys. B* **2022**, *31*, 038101. [CrossRef]
5. Al-badri, K.S.L.; Abdulkarim, Y.L.; Alkurt, F.Ö. Simulated and experimental verification of the microwave dual-band metamaterial perfect absorber based on square patch with a 450 diagonal slot structure. *J. Electromagnet. Wave. App.* **2021**, *35*, 1541–1552. [CrossRef]
6. Abdulkarim, Y.I.; Muhammadsharif, F.F.; Bakır, M.; Awl, H.N. Hypersensitized Metamaterials Based on a Corona-Shaped Resonator for Efficient Detection of Glucose. *Appl. Sci.* **2021**, *11*, 103. [CrossRef]
7. Dincer, F.; Karaaslan, M.; Colak, S.; Tetik, E.; Akgol, O.; Altintas, O.; Sabah, C. Multi-band polarization independent cylindrical metamaterial absorber and sensor application. *Phys. Rev. B* **2016**, *30*, 1650095. [CrossRef]
8. Akinoglu, G.E.; Mir, S.H.; Gatensby, R. Block copolymer derived vertically coupled plasmonic arrays for surface-enhanced Raman spectroscopy. *ACS. Appl. Mater. Interfaces* **2020**, *12*, 23410–23416. [CrossRef]
9. Mir, S.H.; Rydzek, G.; Nagahara, L.A. Erratum: Review—Recent Advances in Block-Copolymer Nanostructured Subwavelength Antireflective Surfaces. *J. Electrochem. Soc.* **2019**, *167*, 037502. [CrossRef]

10. Landy, N.L.; Sajuyigbe, S.; Mock, J.J.; Smith, D.R. Perfect metamaterial absorber. *Phys. Rev. Lett.* **2008**, *100*, 207402. [CrossRef]
11. Wu, B.; Liu, Z.; Du, G.; Chen, Q.; Liu, X.; Fu, G.; Liu, G. Polarization and angle insensitive ultra-broadband mid-infrared perfect absorber. *Phys. Lett. A* **2020**, *384*, 126288. [CrossRef]
12. Wang, J.X.; Cheng, Y.Z.; Luo, H.; Chen, F.; Wu, L. High-gain bidirectional radiative circularly polarized antenna based on focusing metasurface. *Int. J. Electron. Commun.* **2022**, *151*, 154222. [CrossRef]
13. Behera, S.; Fry, P.W.; Francis, H. Broadband, wide-angle antireflection in GaAs through surface nano-structuring for solar cell applications. *Sci. Rep.* **2020**, *10*, 6269. [CrossRef]
14. Zhu, X.Z.; Cheng, Y.Z.; Fan, J.P.; Chen, F.; Luo, H.; Wu, L. Switchable efficiency terahertz anomalous refraction and focusing based on graphene metasurface. *Diam. Relat. Mater.* **2022**, *121*, 108743. [CrossRef]
15. Sun, K.; Xiao, W.; Wheeler, C.; Simeoni, M.; Urbani, A. VO_2 metasurface smart thermal emitter with high visual transparency for passive radiative cooling regulation in space and terrestrial applications. *Nanophotonics* **2022**. [CrossRef]
16. Gunduz, O.T.; Sabah, C. Polarization angle independent perfect multiband metamaterial absorber and energy harvesting application. *J. Comput. Electron.* **2016**, *15*, 228–238. [CrossRef]
17. Nakanishi, T.; Kitano, M. Implementation of electromagnetically induced transparency in a metamaterial controlled with auxiliary waves. *Phys. Rev. Appl.* **2015**, *4*, 024013. [CrossRef]
18. Cheng, T.T.; Gao, H.J.; Liu, G.R.; Pu, Z.S.; Wang, S.F.; Yi, Z.; Wu, X.; Yang, H. Preparation of core-shell heterojunction photocatalysts by coating CdS nanoparticles onto $Bi_4Ti_3O_{12}$ hierarchical microspheres and their photocatalytic removal of organic pollutants and Cr(VI) ions. *Colloids Surf. A Physicochem. Eng. Asp.* **2021**, *633*, 127918. [CrossRef]
19. Lin, X.; Li, Y.J.; Chen, F.T.; Xu, P.; Li, M. Facile synthesis of mesoporous titanium dioxide doped by Ag-coated graphene with enhanced visible-light photocatalytic performance for methylene blue degradation. *RSC Adv.* **2017**, *7*, 25314–25324. [CrossRef]
20. Li, L.X.; Gao, H.J.; Liu, G.R.; Wang, S.F.; Yi, Z.; Wu, X.W.; Yang, H. Synthesis of carnation flower-like $Bi_2O_2CO_3$ photocatalyst and its promising application for photoreduction of Cr(VI). *Adv. Powder Technol.* **2022**, *33*, 103481. [CrossRef]
21. Li, L.X.; Gao, H.J.; Yi, Z.; Wang, S.F.; Wu, X.W.; Li, R.S.; Yang, H. Comparative investigation on synthesis, morphological tailoring and photocatalytic activities of $Bi_2O_2CO_3$ nanostructures. *Colloids Surf. A Physicochem. Eng. Asp.* **2022**, *644*, 128758. [CrossRef]
22. Tang, N.; Li, Y.; Chen, F.; Han, Z. In situ fabrication of a direct Z-scheme photocatalyst by immobilizing CdS quantum dots in the channels of graphene-hybridized and supported mesoporous titanium nanocrystals for high photocatalytic performance under visible light. *RSC Adv.* **2018**, *8*, 42233–42245. [CrossRef] [PubMed]
23. Li, L.X.; Sun, X.F.; Xian, T.; Gao, H.J.; Wang, S.F.; Yi, Z.; Wu, X.W.; Yang, H. Template-free synthesis of $Bi_2O_2CO_3$ hierarchical nanotubes self-assembled from ordered nanoplates for promising photocatalytic application. *Phys. Chem. Chem. Phys.* **2022**, *24*, 8279–8295. [CrossRef]
24. Rosenberg, J.; Shenoi, R.V.; Vandervelde, T.E. A multispectral and polarization-selective surface-plasmon resonant midinfrared detector. *Appl. Phys. Lett.* **2009**, *95*, 161101. [CrossRef]
25. Zhou, F.; Qin, F.; Yi, Z.; Yao, W.T.; Liu, Z.; Wu, X.; Wu, P. Ultra-wideband and wide-angle perfect solar energy absorber based on Ti nanorings surface plasmon resonance. *Phys. Chem. Chem. Phys.* **2021**, *23*, 17041–17048. [CrossRef] [PubMed]
26. Cheng, Y.; Yu, J.; Li, X. Tri-band high-efficiency circular polarization convertor based on double-split-ring resonator structures. *Appl. Phys. B* **2022**, *128*, 1. [CrossRef]
27. Zheng, Z.P.; Zheng, Y.; Luo, Y.; Yi, Z.; Zhang, J.G.; Liu, Z.M.; Yang, W.X.; Yu, Y.; Wu, X.W.; Wu, P.H. Switchable terahertz device combining ultra-wideband absorption and ultra-wideband complete reflection. *Phys. Chem. Chem. Phys.* **2022**, *24*, 2527–2533. [CrossRef]
28. Baqir, M.A.; Choudhury, P.K. Design of hyperbolic metamaterial-based absorber comprised of Ti nanospheres. *IEEE. Photon. Technol. Lett.* **2019**, *31*, 735–738. [CrossRef]
29. Wu, X.; Zheng, Y.; Luo, Y.; Zhang, J.; Yi, Z.; Wu, X.; Cheng, S.; Yang, W.; Yu, Y.; Wu, P. A four-band and polarization-independent BDS-based tunable absorber with high refractive index sensitivity. *Phys. Chem. Chem. Phys.* **2021**, *23*, 26864–26873. [CrossRef]
30. Farsinezhad, S.; Shanavas, T.; Mahdi, N. Core-shell titanium dioxide-titanium nitride nanotube arrays with near-infrared plasmon resonances. *Nanotechnology* **2018**, *29*, 154006. [CrossRef]
31. Xiong, S.; Yin, Z.; Zhou, Y.; Peng, X.; Yan, W.; Liu, Z.; Zhang, X. The dual-frequency (20/40 kHz) ultrasound assisted photocatalysis with the active carbon fiber-loaded Fe^{3+}-TiO_2 as photocatalyst for degradation of organic dye. *Bull. Korean Chem. Soc.* **2013**, *34*, 3039–3045. [CrossRef]
32. Li, Y.; Li, M.; Xu, P.; Tang, S.; Liu, C. Efficient photocatalytic degradation of acid orange 7 over N-doped ordered mesoporous titania on carbon fibers under visible-light irradiation based on three synergistic effects. *Appl. Catal. A Gen.* **2016**, *524*, 163–172. [CrossRef]
33. Zheng, Y.; Wu, P.H.; Yang, H.; Yi, Z.; Luo, Y.; Liu, L.; Song, Q.J.; Pan, M.; Zhang, J.G.; Cai, P.G. High efficiency Titanium oxides and nitrides ultra-broadband solar energy absorber and thermal emitter from 200 nm to 2600 nm. *Opt. Laser Technol.* **2022**, *150*, 108002. [CrossRef]
34. Zhao, F.; Lin, J.C.; Lei, Z.H.; Yi, Z.; Qin, F.; Zhang, J.G.; Liu, L.; Wu, X.W.; Yang, W.X.; Wu, P.H. Realization of 18.97% Theoretical Efficiency of 0.9 μm Thick c-Si/ZnO Heterojunction Ultrathin-film Solar Cells via Surface Plasmon Resonance Enhancement. *Phys. Chem. Chem. Phys.* **2022**, *24*, 4871–4880. [CrossRef] [PubMed]
35. Perrakis, G.; Tasolamprou, A.D.; Kenanakis, G. Submicron Organic–Inorganic Hybrid Radiative Cooling Coatings for Stable, Ultrathin and Lightweight Solar Cells. *ACS Photon.* **2022**, *9*, 1327–1337. [CrossRef]

36. Park, S.; Heo, S.W.; Lee, W. Self-powered ultra-flexible electronics via nano-grating-patterned organic photovoltaics. *Nature* **2018**, *561*, 516–521. [CrossRef]
37. Taflove, A.; Hagness, S.C. *Computational Electrodynamics: The Finite-Difference Time-Domain Method*; Artech House: Boston, MA, USA, 2000.
38. Chen, H.; Chen, Z.H.; Yang, H.; Wen, L.H.; Yi, Z.; Zhou, Z.G.; Dai, B.; Zhang, J.G.; Wu, X.W.; Wu, P.H. Multi-mode surface plasmon resonance absorber based on dart-type single-layer graphene. *RSC Adv.* **2022**, *12*, 7821–7829. [CrossRef]
39. Deng, Y.; Cao, G.; Wu, Y.; Zhou, X.; Liao, W. Theoretical Description of Dynamic Transmission Characteristics in MDM Waveguide Aperture-Side-Coupled with Ring Cavity. *Plasmonics* **2015**, *10*, 1537–1543. [CrossRef]
40. Liu, Y.; Bo, M.; Yang, X.; Zhang, P.; Sun, C.Q.; Huang, Y. Size modulation electronic and optical properties of phosphorene nanoribbons: DFT–BOLS approximation. *Phys. Chem. Chem. Phys.* **2017**, *19*, 5304–5309. [CrossRef]
41. Cai, L.; Zhang, Z.; Xiao, H.; Chen, S.; Fu, J. An eco-friendly imprinted polymer based on graphene quantum dots for fluorescent detection of p-nitroaniline. *RSC Adv.* **2019**, *9*, 41383–41391. [CrossRef]
42. Long, F.; Zhang, Z.H.; Wang, J.; Yan, L.; Lu, P.P.; Yang, Z.X. Magnetic graphene modified imprinted electrochemical sensor for detection of 4-Octylphenol. *Chin. J. Anal. Chem.* **2016**, *44*, 908–914.
43. Li, J.; Jiang, J.; Xu, Z.; Liu, M.; Tang, S.; Yang, C.; Qian, D. Facile synthesis of Ag@Cu_2O heterogeneous nanocrystals decorated N-doped reduced graphene oxide with enhanced electrocatalytic activity for ultrasensitive detection of H_2O_2. *Sens. Actuators B Chem.* **2018**, *260*, 529–540. [CrossRef]
44. Palik, E.D. *Handbook of Optical Constants of Solids II*; Academic Press: Boston, MA, USA, 1991; pp. 77–135.
45. American Society for Testing and Materials (ASTM). Air Mass 1.5 Spectra. Available online: https://rredc.nrel.gov/solar/spectra/am1.5/ (accessed on 13 April 2022).
46. Liu, Z.Q.; Liu, G.; Huang, Z.; Liu, X.; Fu, G. Ultra-broadband perfect solar absorber by an ultra-thin refractory titanium nitride meta-surface. *Sol. Energy Mater. Sol. C* **2018**, *179*, 346–352. [CrossRef]
47. Qian, Q.; Wang, C.; Fan, L.; Cheng, L.; Chen, H.; Zhao, L. An Ultra-Broadband Metasurface Perfect Absorber Based on the triple Mie Resonances. *Opt. Mater.* **2021**, *116*, 111103. [CrossRef]
48. Liu, J.; Ma, W.; Chen, W.; Yu, G.; Chen, Y.; Deng, X.; Yang, C. Numerical analysis of an ultra-wideband metamaterial absorber with high absorptivity from visible light to near-infrared. *Opt. Express* **2020**, *28*, 23748–23760. [CrossRef] [PubMed]
49. Li, J.; Jiang, J.; Zhao, D.; Xu, Z.; Liu, M.; Liu, X.; Tong, H.; Qian, D. Novel hierarchical sea urchin-like Prussian blue@palladium core—Shell heterostructures supported on nitrogen-doped reduced graphene oxide: Facile synthesis and excellent guanine sensing performance. *Electrochim. Acta* **2020**, *330*, 135196. [CrossRef]
50. Cai, R.; Rao, W.; Zhang, Z.; Long, F.; Yin, Y. An imprinted electrochemical sensor for bisphenol A determination based on electrodeposition of a graphene and Ag nanoparticle modified carbon electrode. *Anal. Methods* **2014**, *6*, 1590–1597. [CrossRef]
51. Deng, Y.; Cao, G.; Yang, H.; Zhou, X.; Wu, Y. Dynamic Control of Double Plasmon-Induced Transparencies in Aperture-Coupled Waveguide-Cavity System. *Plasmonics* **2018**, *13*, 345–352. [CrossRef]
52. Zheng, Z.P.; Zheng, Y.; Luo, Y.; Yi, Z.; Zhang, J.G.; Liu, L.; Song, Q.J.; Wu, P.H.; Yu, Y.; Zhang, J.F. Terahertz perfect absorber based on flexible active switching of ultra-broadband and ultra-narrowband. *Opt. Express* **2021**, *29*, 42787–42799. [CrossRef]
53. Long, F.; Zhang, Z.; Wang, J.; Yan, L.; Zhou, B. Cobalt-nickel bimetallic nanoparticles decorated graphene sensitized imprinted electrochemical sensor for determination of octylphenol. *Electrochim. Acta* **2015**, *168*, 337–345. [CrossRef]
54. Cao, G.; Li, H.; Deng, Y.; Zhan, S.; He, Z.; Li, B. Systematic Theoretical Analysis of Selective-Mode Plasmonic Filter Based on Aperture-Side-Coupled Slot Cavity. *Plasmonics* **2014**, *9*, 1163–1169. [CrossRef]
55. Lv, P.; Xie, D.; Zhang, Z. Magnetic carbon dots based molecularly imprinted polymers for fluorescent detection of bovine hemoglobin. *Talanta* **2018**, *188*, 145–151. [CrossRef] [PubMed]
56. Yang, X.; Zhang, F.; Hu, Y.J.; Chen, D.Z.; He, Z.Q.; Xiong, L.Z. Gold nanoparticals doping graphene sheets nanocomposites sensitized screen-printed carbon electrode as a disposable platform for voltammetric determination of guaiacol in bamboo juice. *Int. J. Electrochem. Sci.* **2014**, *9*, 5061–5072.
57. Long, F.; Wang, J.; Zhang, Z.H.; Yan, L. Magnetic imprinted electrochemical sensor combined with magnetic imprinted solid-phase extraction for rapid and sensitive detection of tetrabromobisphenol S. *J. Electroanal. Chem.* **2016**, *777*, 58–66. [CrossRef]
58. Yan, Z.D.; Lu, X.; Du, W.; Lv, Z.Q.; Tang, C.J.; Cai, P.G.; Gu, P.; Chen, J.; Yu, Z. Ultraviolet graphene ultranarrow absorption engineered by lattice plasmon resonance. *Nanotechnology* **2021**, *32*, 465202. [CrossRef]
59. Chen, P.; Liu, F.; Ding, H.; Chen, S.; Chen, L.; Li, Y.-J.; Au, C.-T.; Yin, S.-F. Porous double-shell CdS@C3N4 octahedron derived by in situ supramolecular self-assembly for enhanced photocatalytic activity. *Appl. Catal. B Environ.* **2019**, *252*, 33–40. [CrossRef]
60. Cheng, Z.; Liao, J.; He, B.; Zhang, F.; Zhang, F.; Huang, X.; Zhou, L. One-Step Fabrication of Graphene Oxide Enhanced Magnetic Composite Gel for Highly Efficient Dye Adsorption and Catalysis. *ACS Sustain. Chem. Eng.* **2015**, *3*, 1677–1685. [CrossRef]
61. Li, J.; Chen, X.; Yi, Z.; Yang, H.; Tang, Y.; Yi, Y.; Yao, W.; Wang, J.; Yi, Y. Broadband solar energy absorber based on monolayer molybdenum disulfide using tungsten elliptical arrays. *Mater. Today Energy* **2020**, *16*, 100390. [CrossRef]
62. Chen, H.-J.; Zhang, Z.-H.; Cai, R.; Kong, X.-Q.; Chen, X.; Liu, Y.-N.; Yao, S.-Z. Molecularly imprinted electrochemical sensor based on a reduced graphene modified carbon electrode for tetrabromobisphenol A detection. *Analyst* **2013**, *138*, 2769–2776. [CrossRef]
63. Zhang, Z.; Cai, R.; Long, F.; Wang, J. Development and application of tetrabromobisphenol A imprinted electrochemical sensor based on graphene/carbon nanotubes three-dimensional nanocomposites modified carbon electrode. *Talanta* **2015**, *134*, 435–442. [CrossRef]

64. Liu, H.; Wang, Q.; Zhang, F. Preparation of Fe_3O_4@SiO_2@P(AANa-co-AM) composites and their adsorption for Pb (II). *ACS Omega* **2020**, *5*, 8816–8824. [CrossRef]
65. Yi, Z.; Li, J.; Lin, J.; Qin, F.; Chen, X.; Yao, W.; Liu, Z.; Cheng, S.; Wu, P.; Li, H. Broadband polarization-insensitive and wide-angle solar energy absorber based on tungsten ring-disc array. *Nanoscale* **2020**, *12*, 23077–23083. [CrossRef] [PubMed]
66. Ghobadi, A.; Hajian, H.; Gokbayrak, M.; Dereshgi, S.A. Visible light nearly perfect absorber, an optimum unit cell arrangement for near absolute polarization insensitivity. *Opt. Express* **2017**, *25*, 27624–27634. [CrossRef]
67. Zhang, C.; Yi, Y.; Yang, H.; Yi, Z.; Chen, X.F.; Zhou, Z.G.; Yi, Y.G.; Li, H.L.; Chen, J.; Liu, C. Wide spectrum solar energy absorption based on germanium plated ZnO nanorod arrays: Energy band regulation, Finite element simulation, Super hydrophilicity, Photothermal conversion. *Appl. Mater. Today* **2022**, *28*, 101531. [CrossRef]
68. Qin, C.Y.; Kim, J.B.; Gonome, H. Absorption characteristics of nano-particles with sharp edges for a direct-absorption solar collector. *Renew. Energy* **2020**, *145*, 21–28. [CrossRef]